8 Grain Boundary Diffusion in Metals

Christian Herzig and Yuri Mishin

8.1 Introduction

Grain boundary (GB) diffusion plays an important role in many processes taking place in engineering materials at elevated temperatures. Such processes include Coble creep, sintering, diffusion-induced grain boundary migration, discontinuous reactions (such as discontinuous precipitation, discontinuous coarsening, etc.), recrystallization, and grain growth. GB diffusion is important not only at high temperatures but sometimes also at relatively low, even ambient temperatures. In particular, the service life of many microelectronic elements and devices is limited by room temperature diffusion or electromigration of detrimental impurities along GBs resulting in the degradation of service characteristics.

The fact that GBs provide high diffusivity ("short circuit") paths in metals has been known since a few decades. First indications of enhanced atomic mobility at GBs were obtained as early as in the 1920–1930s, for example from grain size dependence of creep and sintering rates in polycrystalline materials. However, the first direct proof of GB diffusion was obtained in the early 1950s using autoradiography [1]: the additional blackening of autoradiographic images along GBs indicated that the radiotracer atoms penetrated into GBs much faster than in the regular lattice [2]. These observations were immediately followed by two important events: the appearance of the nowadays classic Fisher model of boundary diffusion [3], on one hand, and the development and extensive use of the radiotracer serial sectioning technique, on the other hand. It was largely due to these events that GB diffusion studies were put on a quantitative basis and GB diffusion measurements became the subject of many investigations and publications. Over the five decades that followed, the experimental techniques for GB diffusion measurements have been drastically improved and extended to a wide range of temperatures and a broad spectrum of metallic, semiconductor, and ceramic materials. On the theoretical side, the Fisher model, being still the footing stone of GB diffusion theory, has been subject to careful mathematical analysis and extended to various situations encountered in diffusion experiments and technological processes. For an overview of both fundamentals and recent achievements in this area see the book of Kaur et al. [4] and review articles [5–7]. A com-

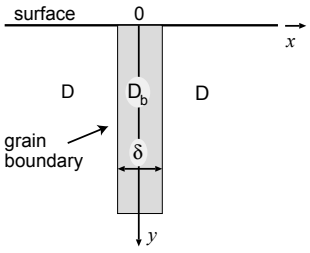

Fig. 8.1. Schematic geometry of the Fisher model of grain boundary diffusion.

plete collection of experimental data published before the end of 1980s can be found in the handbook of Kaur et al. [8].

This chapter presents a brief review of fundamental aspects of GB diffusion with emphasis on metals and metallic alloys. In Sects. 8.2 and 8.3 we introduce classifications of GB diffusion kinetics and mathematical models applied for the analysis of experimental concentration profiles. We also give a brief summary of the current knowledge of GB diffusion in metals. In Sect. 8.4 we discuss in more detail the problem of GB diffusion accompanied by GB segregation and discuss the recent progress in this area. In Sect. 8.5 we summarize. The idea which we wish to emphasize in this review is that many problems in this area could only be solved by combining new theoretical models with precise measurements using novel experimental techniques.

8.2 Fundamentals of Grain Boundary Diffusion

8.2.1 Basic Equations of Grain Boundary Diffusion

Most mathematical treatments of GB diffusion are based on the Fisher model [3] describing diffusion along a single GB. In the Fisher model, a GB is represented as a high-diffusivity uniform and isotropic slab embedded in a low-diffusivity isotropic crystal perpendicular to its surface (Fig. 8.1). The GB is thus described by two physical parameters: the GB width δ and the GB diffusion coefficient D_b such that $D_\mathrm{b} \gg D$, D being the volume diffusion coefficient. In a typical diffusion experiment, a layer of foreign atoms or tracer atoms of the same material is created at the surface and the specimen is annealed at a constant temperature T for a time t. During the anneal the atoms diffuse from the surface into the specimen in two ways: directly into the grains and, much faster, along the GB. In turn, the atoms which diffuse along the GB eventually leave it and continue to diffuse in the lattice regions adjacent to the GB, thus giving rise to a volume diffusion field around the GB.

Mathematically, the diffusion process is described by two coupled equations:

$$\frac{\partial c}{\partial t} = D\left(\frac{\partial^2 c}{\partial x^2} + \frac{\partial^2 c}{\partial y^2}\right), \qquad \text{where } |x| > \delta/2, \tag{8.1}$$

$$\frac{\partial c_\mathrm{b}}{\partial t} = D_\mathrm{b}\frac{\partial^2 c_\mathrm{b}}{\partial y^2} + \frac{2D}{\delta}\left(\frac{\partial c}{\partial x}\right)_{x=\delta/2}. \tag{8.2}$$

These equations represent diffusion in the volume and along the GB, respectively. $c(x, y, t)$ is the volume concentration of the diffusing atoms and $c_\mathrm{b}(y, t)$ is their concentration in the GB. The second term in the right-hand side of (8.2) takes into account the leakage of the diffusing atoms from the GB to the volume. Any solution of (8.1) and (8.2) should meet the surface condition, which can be different in different experiments (see below), as well as the natural initial and boundary conditions at $x \to \pm\infty$ and $y \to \infty$. The joining condition between functions $c(x, y, t)$ and $c_\mathrm{b}(y, t)$ depends on whether we study self-diffusion or impurity diffusion. For self-diffusion, the joining condition simply reflects the continuity of the concentration across the GB,

$$c_\mathrm{b}(y, t) = c(\pm\delta/2, y, t). \tag{8.3}$$

For impurity diffusion, the joining condition involves the equilibrium segregation factor s and reads

$$c_\mathrm{b}(y, t) = sc(\pm\delta/2, y, t). \tag{8.4}$$

The physical meaning of this relation will be discussed later.

8.2.2 Surface Conditions

Fisher [3] postulated a constant source condition at the surface,

$$c(x, 0, t) = c_0 = \text{const}. \tag{8.5}$$

This condition is also called a thick-layer condition because it can be established by depositing a thick layer of diffusant, $h \gg (Dt)^{1/2}$. The constant source condition also applies when diffusion takes place from a gas phase.

Later Suzouka [9, 10] introduced an instantaneous source, or thin-layer condition,

$$c(x, y, 0) = M\delta(y), \qquad (\partial c/\partial y)_{y=0} = 0, \tag{8.6}$$

where M is the amount of diffusant deposited per unit area of the surface. This surface condition assumes that the initial layer is completely consumed by the specimen during the diffusion experiment, i.e. $h \ll (Dt)^{1/2}$. Note that (8.6) unrealistically assumes that the rate of surface diffusion is the same as the rate of volume diffusion, which contradicts existing experimental data.

A more realistic thin-layer condition, called fast surface diffusion condition, was proposed in [4, 11]. That condition postulates that surface diffusion is much faster than volume and even GB diffusion, which results in a uniform

surface concentration near the GB-surface intersect. The respective surface condition is

$$c(x, y, 0) = M\delta(y), \qquad c(x, 0, t) = M/(\pi Dt)^{1/2}. \tag{8.7}$$

This condition also assumes that $h \ll (Dt)^{1/2}$.

In modern experiments thin-layer conditions are established more often than the constant source condition. This is due to the use of extremely thin radiotracer layers which do not disturb the structural or chemical state of GBs in the course of the diffusion experiment.

8.2.3 Methods of Profile Analysis

The basic equations of the Fisher model, (8.1) and (8.2), can be solved analytically. The integral representations of the exact solutions for the constant and instantaneous sources were derived by Whipple [12] and Suzuoka [9, 10], respectively. Using the same Fourier-Laplace transformation method, the exact analytical solution was also obtained for the fast surface diffusion condition, (8.7) [4]. Unfortunately, the practical significance of exact solutions is very limited because of their very complicated mathematical form. In practical terms, any mathematical solution is only useful if it offers a way to process the experimental concentration profile and determine GB diffusion characteristics.

GB diffusion measurements typically employ the radiotracer serial sectioning method. After the diffusion anneal, thin-layers of the material parallel to the source surface are removed from the specimen (either mechanically or by ion beam sputtering) and the radioactivity of each section is measured with a crystalline γ-detector or a liquid scintillation counter. Experimental details of this method can be found in the literature [13, 14], see also Chap. 1. The quantity measured by this method is the average layered concentration of the diffusant, $\overline{c}$, as a function of the penetration depth y. This function, called a concentration (or penetration) profile, bears information about GB diffusion parameters and is therefore subject to a mathematical treatment with the purpose of extracting that information. Much work has been devoted to the development of approximate analytical solutions of the Fisher model and simple recipes of profile analysis.

Fisher [3] derived the following approximate solution for self-diffusion from a constant source:

$$\overline{c} \propto c_0 \exp(-\pi^{-1/4} w), \tag{8.8}$$

where the precise value of the proportionality constant is not important. Here w is the reduced penetration depth defined by

$$w = \frac{y}{(\delta D_{\mathrm{b}})^{1/2}} \left(\frac{4D}{t}\right)^{1/4}. \tag{8.9}$$

Equation (8.8) suggests that the penetration profile $\overline{c}(y)$ plotted in the coordinates $\log \overline{c}$ versus y should yield a straight line. Then, knowing the slope $\partial \ln \overline{c}/\partial y$ of that line we can determine the product δD_b:

$$\delta D_\mathrm{b} = 1.128(D/t)^{1/2}(-\partial \ln \overline{c}/\partial y)^{-2}. \tag{8.10}$$

The volume diffusion coefficient D is assumed to be known from independent measurements.

Fisher's exponential solution, (8.8), is not very accurate. If a profile calculated using Whipple's [12] exact analytical solution is plotted in the coordinates $\log \overline{c}$ versus y^n with various powers n, the best straight line is obtained with the power of $n = 6/5$ [15, 16]. Moreover, the linear part of the profile scales with the reduced depth w defined by (8.9) with a constant slope of about -0.78:

$$\frac{\partial \ln \overline{c}}{\partial w^{6/5}} \approx -0.78. \tag{8.11}$$

It immediately follows that, knowing the slope of the experimental profile in the coordinates $\log \overline{c}$ versus $y^{6/5}$, we can calculate the product δD_b:

$$\delta D_\mathrm{b} = 1.322(D/t)^{1/2}\left(-\partial \ln \overline{c}/\partial y^{6/5}\right)^{-5/3}. \tag{8.12}$$

Equations (8.11) and (8.12) are only valid under two conditions:

- The so-called LeClaire's parameter β defined by
$$\beta = \frac{\delta D_\mathrm{b}}{2D(Dt)^{1/2}} \tag{8.13}$$
must be large enough, in practical conditions $\beta > 10$.
- Parameter
$$\alpha = \frac{\delta}{2(Dt)^{1/2}} \tag{8.14}$$
must be small enough, in practical conditions $\alpha < 0.1$.

Similarly, for diffusion from an instantaneous source it was found that

$$\frac{\partial \ln \overline{c}}{\partial w^{6/5}} \approx -0.775 \tag{8.15}$$

provided that α is small enough and $\beta > 10^4$ [9, 10]. Therefore, the product δD_b can be determined from the linear part of the profile $\log \overline{c}$ versus $y^{6/5}$:

$$\delta D_\mathrm{b} = 1.308(D/t)^{1/2}\left(-\partial \ln \overline{c}/\partial y^{6/5}\right)^{-5/3}. \tag{8.16}$$

If $\beta < 10^4$, the right-hand side of (8.15) is no longer constant; instead, it becomes a function of β (and thus time). Then, (8.16) should be slightly modified to become

$$\delta D_\mathrm{b} = 1.206(D^{0.585}/t^{0.605})^{1/1.19}\left(-\partial \ln \overline{c}/\partial y^{6/5}\right)^{-5/2.975} \tag{8.17}$$

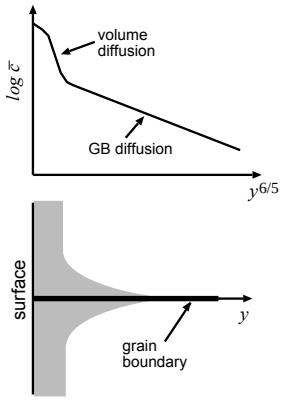

Fig. 8.2. Schematic shape of a typical penetration profile of grain boundary diffusion. If $\alpha \ll 1$ and $\beta \gg 1$, where α and β are defined by (8.13) and (8.14), then the tail of the profile is a straight line in the coordinates $\log \overline{c}$ versus $y^{6/5}$.

for $10^2 < \beta < 10^4$, and

$$\delta D_{\mathrm{b}} = 1.084 (D^{0.91}/t^{1.03})^{1/1.94} \left(-\partial \ln \overline{c}/\partial y^{6/5}\right)^{-5/2.91} \tag{8.18}$$

for $10 < \beta < 10^2$.

The preceding relations describe only one part of the profile, namely, the part which is dominated by GB diffusion. The overall penetration profile typically consists of two parts as shown schematically in Fig. 8.2:

- A near-surface region caused by direct volume diffusion from the surface. The concentration in this region follows a Gaussian function or an error function, depending on the surface condition. If measured accurately, this part can be used to determine the volume diffusion coefficient.
- A long-penetration tail caused by the simultaneous GB diffusion and lateral volume diffusion from the GB to the adjacent grains. It is this tail that should become a straight line when plotted as $\log \overline{c}$ versus $y^{6/5}$. The slope of this line is used to determine the GB diffusivity.

It should be pointed out that the power $n = 6/5$ has no physical meaning and cannot be derived analytically. It simply provides a good numerical approximation of the exact profile in a convenient concentration range and is therefore widely used for the analysis of experimental profiles. A slightly more accurate value of n can be obtained for each particular surface condition or GB geometry in the sample [17]. The obtained values range from 1.1 to 1.2, i.e. are rather close to 6/5. Given the scatter of data points on experimental profiles, the use of one universal power $n = 6/5$ and thus (8.12), (8.16)-(8.18) is a well-justified procedure for all practical purposes. Carefully measured experimental profiles do follow the $y^{6/5}$-rule in a wide concentration range, see examples in Fig. 8.3. Moreover, the linearity of $\log \overline{c}$ versus $y^{6/5}$ is often used as a proof of predominant GB diffusion in the sample and a measure of the profile quality.

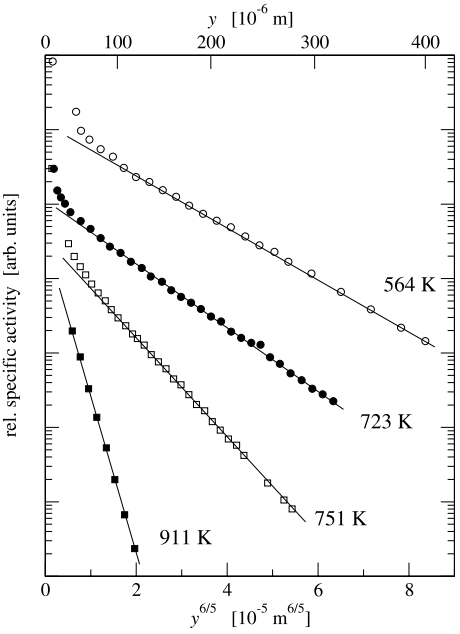

Fig. 8.3. Penetration profiles for self-diffusion in polycrystalline silver [23]. This diagram demonstrates that the GB-related tail of high quality profiles becomes a straight line when plotted as $\log \overline{c}$ versus $y^{6/5}$.

Equations (8.12), (8.16)-(8.18) are only valid for self-diffusion in metals. The case of impurity diffusion was first analyzed by Bokshtein et al. [18] and Gibbs [19] and later revisited by other authors (see [4] for references). It has been shown that, provided the segregation factor s is a constant, all solutions of the Fisher model remain the same as for self-diffusion except that δ should be replaced by the product $s\delta$. In particular, (8.12), (8.16)-(8.18) should be modified by replacing their left-hand side by $s\delta D_{\mathrm{b}}$. After this modification they can be applied for the determination of the triple product $s\delta D_{\mathrm{b}}$ of impurity diffusion.

8.2.4 What Do We Know About Grain Boundary Diffusion?

It is not our intention to give a complete answer to this question, especially because many topics in this area are still the subject of debates in the literature. We will focus on facts that appear to be well established and will restrict our discussion to self-diffusion in metals.

The Grain Boundary Width

In the case of self-diffusion we can only determine the product δD_{b}. We thus need to know δ if we want to determine the GB diffusion coefficient D_{b}. The assumption $\delta = 0.5$ nm introduced by Fisher [3] seems to be a good approximation. This value of δ is well-consistent with evaluations of GB width

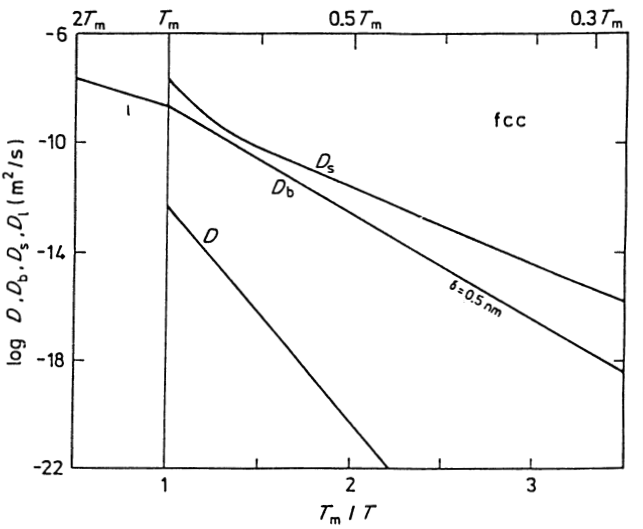

Fig. 8.4. Arrhenius lines for self-diffusion in fcc metals in the lattice (D) [31], along grain boundaries (D_b) [32], on the surface (D_s) [30] and in the liquid phase [30].

by high-resolution transmission electron microscopy, field ion microscopy, and other techniques [4, 20–22]. Furthermore, recent combined B-regime and C-regime measurements (see definitions of these regimes below) of self-diffusion in silver indicate that $\delta = 0.5$ nm is a very good estimate of δ in metals [23,24]. Atomistic computer simulations also confirm that the enhanced diffusivity at GBs is confined to the GB core of around 0.5 nm in thickness [25–29].

Empirical Rules

Like lattice diffusion, GB diffusion normally follows the Arrhenius temperature dependence, $D_\mathrm{b} = D_{\mathrm{b}0} \exp(-Q_\mathrm{b}/RT)$, R being the gas constant. The activation energy Q_b of GB diffusion is about a factor of two smaller than the activation energy Q of lattice diffusion; more exactly, in most metals $Q_\mathrm{b}/Q \approx 0.4$ to 0.6. Typically, GB diffusion is 4 to 8 orders of magnitude

Table 8.1. Empirical correlation between grain boundary self-diffusion and the melting temperature for three classes of metals. T_m is the melting temperature.

	Brown and Ashby [31]		Gust et. al. [32]	
structure	$\delta D_{\mathrm{b}0}$ (m^3/s)	Q_b (J/mol)	$\delta D_{\mathrm{b}0}$ (m^3/s)	Q_b (J/mol)
fcc	9.44×10^{-15}	83.0 T_m	9.7×10^{-15}	75.4 T_m
bcc	3.35×10^{-13}	97.6 T_m	9.2×10^{-15}	86.7 T_m
hcp	2.74×10^{-14}	89.8 T_m	1.5×10^{-14}	85.4 T_m

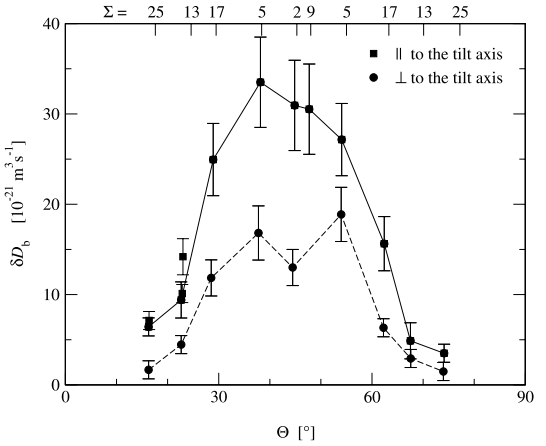

Fig. 8.5. Orientation dependence of self-diffusion in [001] symmetrical tilt grain boundaries in silver at $T = 771\,\mathrm{K}$ [34].

faster than volume diffusion depending on the temperature (Fig. 8.4). This tremendous difference in the diffusion coefficients is mainly due to the difference in the activation energies while the respective pre-exponential factors are close to one another. For all metals, D_b approaches a common value of about 10^{-9} to 3×10^{-9} $\mathrm{m^2 s^{-1}}$ at the melting temperature T_m [30]. Even near the melting point, D_b remains significantly higher than D and approaches the diffusion coefficient in the liquid phase (Fig. 8.4). In Table 8.1 we summarize empirical correlations between GB diffusion data and T_m for three classes of metals (fcc, bcc and hcp) derived by Brown and Ashby [31] and Gust et al. [32]. These correlations offer a good base for the systematics of available GB diffusion data and the evaluation of new data.

Anisotropy of Grain Boundary Diffusion

If diffusion is measured in two mutually perpendicular directions in the same GB, the obtained diffusion coefficients are generally different. The first measurements of this type were performed by Hoffman [33] for self-diffusion along [001] tilt GBs in Ag. He diffused a silver radiotracer into a single GB in silver bicrystals, i.e., samples prepared by the diffusion bonding of two properly oriented single crystals. For small-angle misorientations between the grains the anisotropy was especially strong, with diffusion parallel to the tilt axis ($D_\mathrm{b}^{\parallel}$) being a factor of 15 faster than diffusion perpendicular to the tilt axis ($D_\mathrm{b}^{\perp}$). These observations were explained in terms of the dislocation model of small-angle GBs. However, some anisotropy $D_\mathrm{b}^{\parallel}/D_\mathrm{b}^{\perp} \approx 2$ still remained even when the tilt angle θ became as large as 45°. Since the dislocation model is not valid at large misorientations, the measurements of Hoffman suggest that even large-angle GBs are not amorphous but instead have a well-ordered anisotropic structure. Figure 8.5 shows more recent results of diffusion anisotropy measurements, also in bicrystals with a [001] symmet-

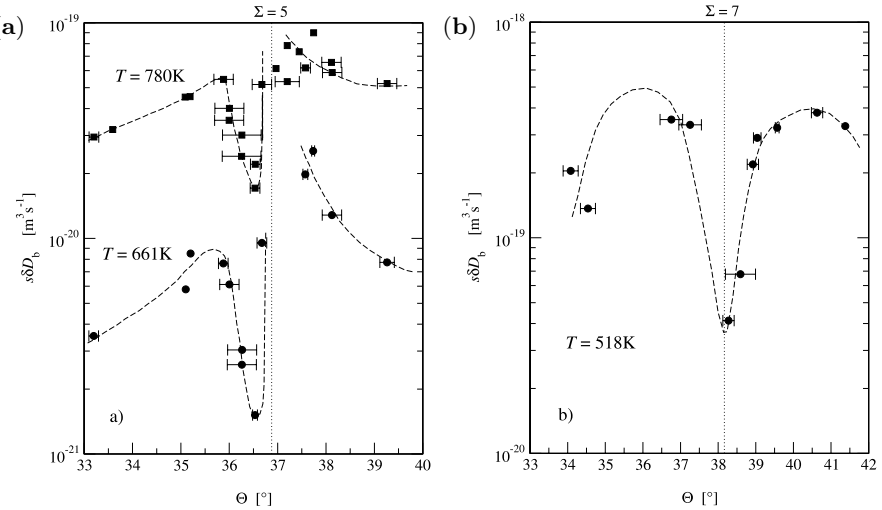

Fig. 8.6. (a) Orientation dependence of ^{195}Au diffusion in [001] symmetrical tilt grain boundaries in Cu measured on oriented bicrystals around the $\Sigma = 5$ (310)[111] orientation [36]. The grain boundary diffusivity $P = s\delta D_{\mathrm{b}}$ is plotted as a function of the tilt angle θ. (b) orientation dependence of Ge diffusion in Al bicrystals around the $\Sigma = 7$ (321)[111] orientation [38].

rical tilt GB in Ag, in the range of high-angle misorientations [34]. Similar results were obtained in other metallic systems [4]. Atomistic computer simulations also predict a significant anisotropy of GB diffusion in metals [26,27].

Orientation Dependence of Grain Boundary Diffusion

If the lattice misorientation between two grains changes continuously and GB diffusion is measured along a fixed direction in the GB plane (e.g., parallel to the tilt axis), will the diffusion characteristics change monotonically or will they show maxima or minima at some special orientations? The first attempt to answer this question was made in the pioneering work of Turnbull and Hoffman [35], again on bicrystals with a [001] symmetrical tilt GB in Ag. They studied only small-angle GBs and found a monotonic increase in the diffusivity with the misorientation angle. Later measurements on large-angle GBs revealed sharp minima at some misorientations with low values of Σ (reciprocal density of coincident sites). For example, Budke et al. [36,37] have studied tracer self-diffusion and Au impurity diffusion in a series of well-characterized Cu GBs in a narrow range ($\Delta\theta = 6°$) of tilt angles around the $\Sigma 5$ (310)[001] symmetrical tilt misorientation. The diffusivity showed a minimum and the activation energy a maximum very close to the perfect $\theta = 36.9°$ misorientation (Fig. 8.6(a)). Similar minima of GB diffusivity were observed for Ge tracer diffusion along the $\Sigma 7$ (321)[111] GB in Al [38] (Fig. 8.6(b)), as well

as for Zn chemical diffusion along the $\Sigma 5$ (310)[001], $\Sigma 9$ (122)[011], and $\Sigma 7$ (321)[111] symmetrical tilt GBs in Al [39]. At first sight, these observations stand in contrast with the continuous orientation dependencies found earlier on [001] symmetrical tilt GBs in Ni [40] and Ag [34, 41] (cf. Fig. 8.5). However, if the minima of D_{b} are confined to narrow ranges around some special misorientations, as was observed in [36–38], they could have been overlooked in the previous studies [34, 40, 41] where the measurements were taken in every 5–7°.

Atomistic Mechanisms of Grain Boundary Diffusion

There is experimental evidence suggesting that GB diffusion in metals and metallic systems takes place by the vacancy mechanism [4, 20, 42]. However, alternative mechanisms cannot be excluded, especially the interstitial mechanism. Recent atomistic computer simulations [25–27, 43] suggest that the full description of GB diffusion should include both the vacancy and interstitial-related mechanisms. Simulations also reveal that vacancies can move by "long jumps" involving a simultaneous displacement of two or more atoms [26, 27]. Interstitials move by the interstitialcy mechanism in which two or more atoms jump in a concerted manner. On some (although rare) occasions even the ring mechanism was found to operate in certain GBs [26]. Which mechanism dominates the overall atomic transport depends on the particular GB structure. Atomistic modeling also suggests that at high temperatures GBs can develop a significantly disordered, "liquid-like" structure [28, 29]. Diffusion in such GBs is believed to occur by mechanisms similar to those in liquids.

8.3 Classification of Diffusion Kinetics

GB diffusion is a complex process involving several elementary processes, such as direct volume diffusion from the surface, diffusion along the GBs, partial leakage of the diffusant from the GBs to the volume, and the subsequent volume diffusion around the GBs. In a polycrystalline material, diffusion transport between individual GBs can also play an important role. Depending on the relative importance of these elementary processes, essentially different diffusion regimes, or kinetics, can occur. In each particular regime one or two elementary processes control the overall rate of diffusion, whereas other processes are unimportant. Each regime dominates in a certain domain of anneal temperatures, times, grain sizes, and other relevant parameters. The knowledge of all regimes that can occur is important for both planning diffusion experiments and the interpretation of their results. The shape of the experimental concentration profile depends on the kinetic regime. Furthermore, the diffusion characteristics that can be extracted from the penetration profile also depend on the kinetic regime and should be identified *a priori*.

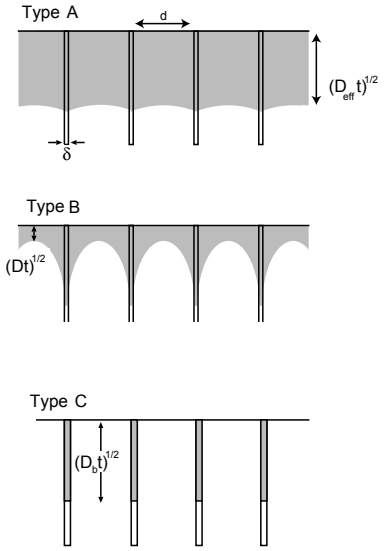

Fig. 8.7. Schematic illustration of type A, B and C diffusion regimes in Harrison's classification.

In this section we consider Harrison's [44] A-B-C classification for a polycrystal containing parallel GBs (Sect. 8.3.1). Some other classifications are discussed in Sect. 8.3.2.

8.3.1 Harrison's Classification

Harrison [44] proposed the first and still the most widely used classification of diffusion kinetics in a polycrystal with parallel GBs. His classification introduces three regimes called type A, type B, and type C (Fig. 8.7).

Type A Kinetics

The A regime is observed at high temperatures, or/and after very long anneals, or/and when the grain size is small. In this regime, the volume diffusion length $(Dt)^{1/2}$ is larger than the spacing d between the GBs, so that volume diffusion fields of neighboring GBs overlap very extensively. Thus, the condition of the A regime is

$$(Dt)^{1/2} \gg d. \tag{8.19}$$

Under this condition an average tracer atom visits many grains and GBs during the anneal time t, which results in planar front diffusion with the penetration depth proportional to $t^{1/2}$. On the macroscopic scale, the polycrystal obeys Fick's law with an effective diffusion coefficient D_{eff}. The latter represents an average of D and D_{b} weighted in the ratio of the number of atomic sites in the grains and in GBs [45],

$$D_{\text{eff}} = fD_{\text{b}} + (1 - f)D \tag{8.20}$$

(Hart's formula). Here f is the volume fraction of GBs in the polycrystal, i.e., $f = q\delta/d$, q being a numerical factor depending on the grain shape ($q = 1$ for parallel GBs). Thus, the experimental penetration profile should follow a Gaussian or an error function solution (depending on the surface condition) with the diffusion coefficient D_{eff}. Since $D_{\text{b}} \gg D$, D_{eff} is generally larger than D, which explains why diffusion coefficients measured on polycrystals are typically higher than the true value of D. If the grain size is large enough, then $f \to 0$ and D_{eff} approaches D. In the other extreme, when d is very small, D_{eff} is dominated by the first term and $D_{\text{eff}} \approx q\delta D_{\text{b}}/d$. Then, knowing the grain size and measuring D_{eff}, we can determine the product δD_{b}.

Type B Kinetics

If the temperature is lower, or/and the diffusion anneal time is shorter, or/and the grain size is larger than in the previous case, then diffusion takes place in the B regime in which

$$\delta \ll (Dt)^{1/2} \ll d. \tag{8.21}$$

As before, GB diffusion is accompanied by volume diffusion around GBs, but volume diffusion fields of neighboring GBs do not overlap (Fig. 8.7). Individual GBs are effectively isolated and mathematical solutions obtained for a single GB (Sect. 8.2) are also valid for a polycrystal. The relation (8.21) also implies that $\alpha \ll 1$. When analyzing the B regime, it is additionally assumed that also $\beta \gg 1$. Under these conditions the penetration profile has a two-step shape (Fig. 8.2) and (8.12), (8.16)-(8.18) can be applied for the profile analysis. The product δD_{b} (for impurity diffusion, $s\delta D_{\text{b}}$) is the only quantity that can be determined in the B regime. This regime comprises the widest and the most convenient temperature range of diffusion measurements in comparison with other regimes.

Type C Kinetics

If, starting from the B regime, we go towards lower temperatures or/and shorter anneal times, we eventually arrive at a situation when volume diffusion is almost "frozen out" and diffusion takes place only along GBs without any leakage to the volume (Fig. 8.7). In this regime, called type C, we have

$$(Dt)^{1/2} \ll \delta, \tag{8.22}$$

and thus $\alpha \gg 1$. The concentration profile is either a Gaussian function

$$\overline{c} \propto \exp\left(-\frac{y^2}{4D_{\text{b}}t}\right) \tag{8.23}$$

(instantaneous source) or an error function

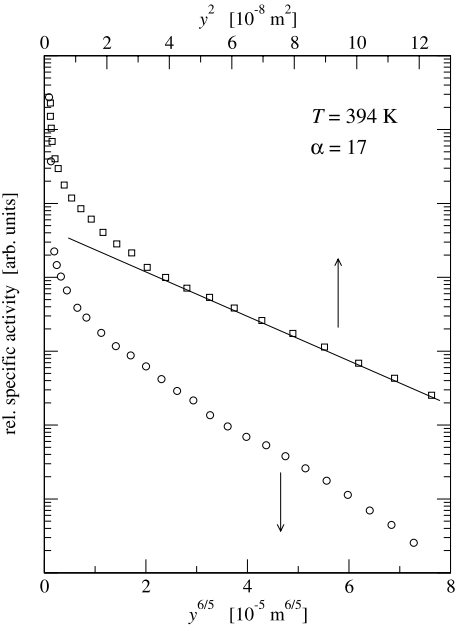

Fig. 8.8. Penetration profile of GB self-diffusion in polycrystalline Ag measured in the C regime ($\alpha = 17$) [23]. In order to measure this profile in a wide concentration range, carrier-free ^{105}Ag radiotracer was implanted at the ISOLDE/CERN facility. After a microtome sectioning, the radioactivities of the sections were determined with a well-type intrinsic Ge γ-detector. The tail of the profile shows a downward curvature when plotted as $\log \overline{c}$ vs $y^{6/5}$ (B-regime format, lower scale) but becomes a straight line when plotted as $\log \overline{c}$ vs y^2 (C-regime format, upper scale).

$$\overline{c} \propto \operatorname{erfc}\left[\frac{y}{2(D_{\mathrm{b}}t)^{1/2}}\right] \tag{8.24}$$

(constant source). If the profile has been measured experimentally (which is extremely difficult to do because the amount of tracer penetrated into the sample is very small), then we can determine D_{b} separately from δ. If the profile has been measured over a wide concentration range, we can distinguish between the B and C regimes already from its shape and not only from the value of α. This fact is illustrated in Fig. 8.8 in which a C-regime profile of GB self-diffusion in Ag is plotted in two different formats [23]. The linearity of the plot $\log \overline{c}$ versus y^2 confirms the C regime.

It is important to know the physical meaning of the parameters α and β used in this classification [4,5]. Parameter α determines the relation between diffusion along the GBs and the leakage of the diffusant from the GBs to the volume. When $\alpha \gg 1$, which is the case in the C regime, then diffusion along the GBs takes place without any leakage to the volume. Then the leakage term in (8.2) can be neglected and this equation is easily solved to give (8.23) and (8.24). If $\alpha \ll 1$ (B regime), the leakage of the diffusant from the GBs is the rate-controlling step while GB diffusion itself is quasi-steady. The latter means that the derivative $\partial c_{\mathrm{b}}/\partial t$ in (8.2) can be neglected, which simplifies this equation and makes the concentration a function of the reduced depth w only.

Parameter β determines the relation between the x and y components of volume diffusion near the GBs. When $\beta \gg 1$ (C and B regimes), volume

diffusion takes place predominantly in the x direction and the term $\partial^2 c/\partial y^2$ in (8.1) can be neglected. This approximation does not apply to the zone of direct volume diffusion near the surface, which is dominated by the term $\partial^2 c/\partial y^2$. However, as long as $\beta \gg 1$, the depth of the direct volume diffusion zone is much smaller than the penetration depth along the GBs. Because β decreases with temperature and time, at high temperatures or after long anneals β becomes small and we arrive at the A regime in which most of the penetration profile lies in the zone of direct volume diffusion.

If the grain size is small, the volume diffusion fields around GBs come to overlap while β is still large. In that case the onset of the A regime is determined by the condition $\Lambda \equiv d/\sqrt{Dt} \ll 1$. Murch and Belova [46] have recently performed kinetic Monte Carlo simulations of GB diffusion across the A and B regimes and established a more practical criterion of the A-B kinetic transition. Namely, the A regime dominates at $\Lambda \leq 0.4$–0.7 (depending on the surface conditions), whereas lower limit of the B regime is $\Lambda \approx 2.0$. The range $0.5 \leq \Lambda \leq 2$ therefore corresponds to the A-B transition kinetics.

Another transient kinetics, namely between the B and C regimes, in which $\alpha \approx 1$, is particularly interesting. It has even been argued that this transition deserves to be treated as separate kinetic regime [4, 11]. In this regime, the diffusion profile depends on both w and α, which opens a possibility to determine both δD_b and δ from the profile shape. Although the respective mathematical treatments have been developed and experimental profiles measured in this transient regime are available in the literature, attempts to determine D_b and δ in such conditions have not been very successful so far [4].

8.3.2 Other Classifications

So far we have only considered a polycrystal with parallel GBs. More realistic models of a polycrystal have been proposed, such as the cubic grain model of Suzuoka [9], the spherical grain model of Bokshtein et al. [18], and the general model of diffusion in isotropic polycrystals by Levine and MacCallum [15]. The spherical grain model has been particularly useful due to its ability to treat diffusion in fine-grained polycrystals. The model was analyzed in several publications and applied to diffusion in fine-grained oxides [47] and growing oxide films [48, 49]. Along with standard regimes that fit into Harrison's classification, both Bokshtein et al. [18] and Levine and MacCallum [15] identified a new regime in which

$$\delta \ll \sqrt{Dt} \ll d \ll L_\mathrm{b}, \tag{8.25}$$

where L_b is the penetration depth along GBs. In this regime the diffusing atoms penetrate to a large depth $L_\mathrm{b} \gg d$ along the GB network but volume diffusion fields around individual GBs still do not overlap. It has been shown [4] that the penetration profile has the same shape as in Harrison's B regime

and that (8.12), (8.16)-(8.18) are still valid, but δ should be replaced by an "effective" GB width $q\delta$, where q is a geometric factor of order unity depending on the grain shape.

A general classification of diffusion kinetics in isotropic polycrystalline materials has been developed in [4, 50]. If the grain size d is allowed to vary over a wide range, a number of new regimes can occur, each defined by a certain relation between the four characteristic lengths involved in the problem: δ, d, $(Dt)^{1/2}$, and L_{b}. In particular, the kinetics defined by (8.25) is one of such regimes. Each regime is characterized by a certain time dependence of the penetration length, a certain shape of the concentration profile, and certain diffusion characteristics that can be determined from the profile. The analysis also shows that all isotropic polycrystals can be divided into three classes called "coarse-grained", "fine-grained", and "ultrafine-grained" polycrystals according to their grain size. Polycrystals of each class exhibit their own set of diffusion regimes. GB segregation has a strong effect on both the concentration profiles and the critical grain sizes separating the three classes of polycrystals. The interested reader is referred to Sect. 2.4.13 of [4] for more details.

Other generalizations of Harrison's classification include the analysis of diffusion in structurally non-uniform GBs [51, 52] and GB diffusion in conditions when the grains are non-uniform [52, 53]. In particular, Klinger and Rabkin [53] proposed an extension of Harrison's classification which recognizes that lattice dislocations, subgrain boundaries, and other extended defects present in the bulk can alter the GB diffusion kinetics. They have identified a new ("type D") regime in which the effective rate of GB diffusion is controlled by short circuit diffusion inside the grains. These and other generalizations are very important as they reach out to more realistic conditions of diffusion experiments and diffusion-controlled processes in materials.

The following example demonstrates the practical usefullness of the analyses of kinetic regimes in polycrystals. Ni GB diffusion in a two-scale material was investigated in [54, 55]. The nanocrystalline γ-Fe–40 wt.%Ni alloy consisted of nanometer-scale grains arranged in micrometer-scale clusters, or agglomerates (cf. Fig. 9.22 in Chap. 9). For the analysis of the complex penetration profiles in this material with two types of short-circuit diffusion paths (the nanocrystalline GBs and the inter-agglomerate interfaces) a further extention of the Harrison classification was suggested [54], which resembles the one introduced in [53]. Diffusion profiles were observed which corresponded to three concurrent processes: (i) Harrison's type B regime of GB diffusion along the nanocrystalline GBs, (ii) type B regime of short-circuit diffusion along the inter-agglomerate boundaries with subsequent outdiffusion into the adjacent nanocrystaline GBs, and finally (iii) volume diffusion (B-B regime). At higher temperatures, when the bulk diffusion fluxes from individual nanocrystalline GBs overlapped, the diffusion process proceeded in the type A regime along the nanocrystalline GBs and in the type B regime along the inter-agglomerate

boundaries with subsequent outdiffusion via combined nanocrystalline GB and bulk diffusion (A-B regime). Mathematical methods for analysing the obtained penetration profiles were also proposed in [54].

8.4 Grain Boundary Diffusion and Segregation

8.4.1 Determination of the Segregation Factor from Grain Boundary Diffusion Data

As mentioned above, GB diffusion experiments are typically performed in the B regime and the measured penetration profiles are analyzed using the $y^{6/5}$-method, see (8.12), (8.16)-(8.18). If we study impurity diffusion, this method gives only the triple product $s\delta D_\mathrm{b}$, the only quantity that can be determined in the B regime. While the GB width δ can be considered as a known constant, $\delta = 0.5$ nm (Sect. 8.2.4), the GB segregation factor s and the GB diffusion coefficient D_b are still to be determined. Because both quantities are essentially temperature dependent and can vary by orders of magnitude, knowing only their product means knowing almost nothing about each of them individually.

In some cases the equilibrium segregation factor s can be determined by independent direct measurements. In direct measurements, the impurity is introduced into the host material and the sample is annealed at a chosen temperature T to let the impurity form an equilibrium GB segregation. The sample is then fractured *in situ* along GBs and the chemical composition of the fracture surface is analyzed using Auger electron spectroscopy or some other surface analytic technique [20–22]. Combining the obtained GB segregation factor with the product $s\delta D_\mathrm{b}$ measured at the same temperature, we can calculate the GB diffusion coefficient D_b. Unfortunately, direct measurements of s are only possible in intrinsically brittle materials, such as ceramics and some intermetallic compounds, and are practically impossible in most of pure metals.

Another way to separate s and D_b is to perform GB diffusion measurements in a wide temperature range covering both B and C regimes. By C regime measurements we can directly determine D_b (Sect. 8.3.1). By combining the obtained D_b values with $s\delta D_\mathrm{b}$ values extrapolated from B regime measurements at high temperatures, we find $s\delta = s\delta D_\mathrm{b}/D_\mathrm{b}$ and thus s assuming $\delta = 0.5$ nm. This approach offers a key to solving two important problems at the same time. Firstly, the GB diffusion coefficients are determined separately. By making systematic measurements of volume and GB diffusion in binary systems, insights can be obtained into mechanisms of GB diffusion and segregation. Secondly, we determine the GB segregation factor and thus the GB segregation energy. That way, diffusion measurements can be used as a tool to study equilibrium GB segregation. This capability

is especially important for non-brittle materials in which direct segregation measurements are not possible.

It should be pointed out that the separate determination of s and D_b from diffusion measurements is based on the following assumptions:

- Local thermodynamic equilibrium is constantly maintained between GBs and the adjacent lattice regions at any depth within the diffusion zone.
- Both volume and GB concentrations of the impurity are small enough to be coupled by the linear equation (8.4) with a constant s. In other words, the GB segregation follows a linear, or Henry-type, isotherm.

A major problem of this approach is that diffusion measurements in the C regime are very difficult. Strong GB segregation favours such measurements by extending the temperature range of the C regime towards higher temperatures. Indeed, since $\alpha = s\delta/2(Dt)^{1/2}$, large s values increase α and allow us to meet the condition $\alpha \gg 1$ at temperatures higher than for self-diffusion. Nevertheless, due to the experimental challenges C regime measurements have practically not been performed until recently even for impurity diffusion. It is only since a few years that reliable and systematic C regime measurements have become possible, mainly due to the use of carrier-free radioisotopes and extremely sensitive γ-detectors with a large counting efficiency and low background. To date, combined B and C regime measurements have been performed in a few systems [56–60]. We will discuss the results for two systems, Te in Ag [56] and Au in Cu [57], which represent the extreme cases of very strong and very weak segregation, respectively.

GB diffusion of Te in Ag was studied in the temperature range 378 to 970 K using the radiotracers ^{123}Te (deposited by vacuum evaporation) and ^{121}Te (carrier-free, implanted at the ISOLDE/CERN facility). Each penetration profile was analyzed in two ways: assuming the B and the C regimes. The actual regime that dominated the experiment was established from the profile shape (whether it became linear in the respective coordinates), and by comparing the α and β values with those required by the B and C regimes. It was found that the B regime prevailed in the temperature range > 600 K (Fig. 8.9). At these temperatures, the $s\delta D_b$ values determined from $\log \overline{c}$ versus $y^{6/5}$ plots followed the Arrhenius relation

$$s\delta D_b = 2.34 \times 10^{-15} \exp\left(-\frac{43.47 \text{ kJ/mol}}{RT}\right) \text{ m}^3/\text{s}. \tag{8.26}$$

It was also established that the measurements below 500 K were dominated by the C regime. At these temperatures the GB diffusion coefficients were determined by fitting the profiles to the Gaussian function. The diffusion coefficients were found to follow the Arrhenius relation

$$D_b = 1.01 \times 10^{-4} \exp\left(-\frac{86.75 \text{ kJ/mol}}{RT}\right) \text{ m}^2/\text{s}. \tag{8.27}$$

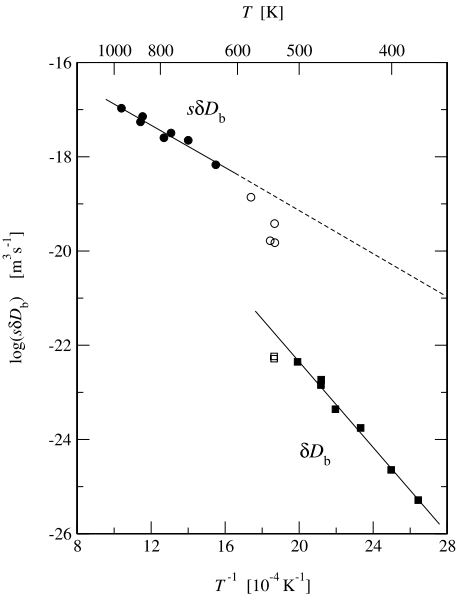

Fig. 8.9. The Arrhenius plot of $s\delta D_\mathrm{b}$ (circles) and δD_b (squares) ($\delta = 0.5$ nm) for Te impurity diffusion along GBs in Ag [56]. The B and C regimes dominate above 600 K and below 500 K, respectively. In the range 500 to 600 K the apparent values of both $s\delta D_\mathrm{b}$ and δD_b are significantly underestimated. The difference between the two Arrhenius lines is due to GB segregation of Te.

In the transition temperature range 500-600 K, the $s\delta D_\mathrm{b}$ and D_b values showed significant downward deviations from the respective Arrhenius lines (Fig. 8.9). This behavior is perfectly consistent with the theoretical analysis [4, 61] and is typical of the transient regime between B and C.

In Fig. 8.9, the δD_b values measured in the C regime are plotted together with $s\delta D_\mathrm{b}$ values extrapolated from the B regime measurements at $T > 600$ K. The difference between the two lines gives the segregation factor s. The high values of s (10^3 to 10^5) are well-consistent with the very small solubility of Te in Ag. The segregation energy determined from the Arrhenius plot of s (Fig. 8.10) equals $E_\mathrm{s} = -43.3$ kJ/mol.

In contrast to the previous case, Au in Cu is a system with complete mutual solubility of the components, so that the GB segregation should be weak. The results of combined B and C regime measurements for this system [57], using the carrier-free radiotracer ^{195}Au, are shown in Fig. 8.11. The Arrhenius relations obtained in the B and C regimes are

$$s\delta D_\mathrm{b} = 2.11 \times 10^{-15} \exp\left(-\frac{81.24 \ \mathrm{kJ/mol}}{RT}\right) \ \mathrm{m}^3/\mathrm{s} \qquad (8.28)$$

and

$$D_\mathrm{b} = 4.87 \times 10^{-6} \exp\left(-\frac{91.03 \ \mathrm{kJ/mol}}{RT}\right) \ \mathrm{m}^2/\mathrm{s}, \qquad (8.29)$$

respectively. The segregation factors s deduced from the diffusion data are shown in Fig. 8.10. As expected, the obtained values of s (8 to 11) and the segregation energy $E_\mathrm{s} = -9.7$ kJ/mol are relatively small. The segregation

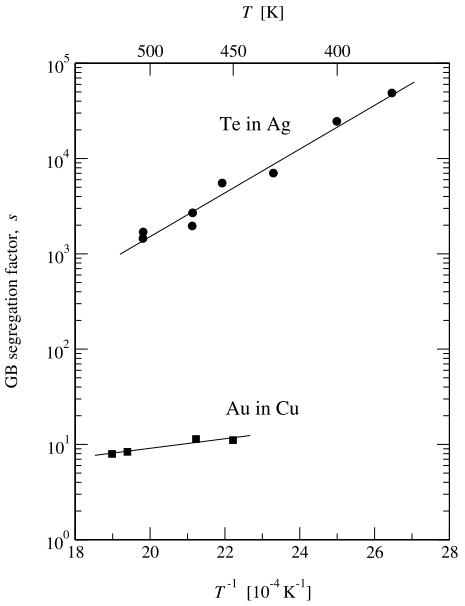

Fig. 8.10. Temperature dependence of the GB segregation factor s of Te in Ag [56] and Au in Cu [57] determined from combined B and C regime measurements.

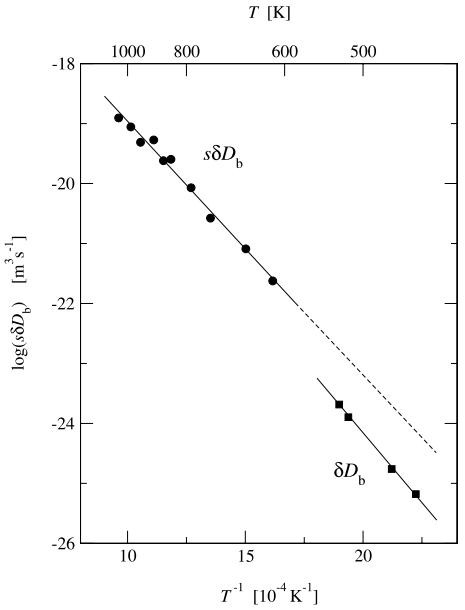

Fig. 8.11. The Arrhenius plot of $s\delta D_\mathrm{b}$ (circles) and δD_b (squares) ($\delta = 0.5$ nm) for Au impurity diffusion along GBs in Cu [57]. The B and C regimes prevail above 618 K and below 526 K, respectively. The difference between the two Arrhenius lines is due to GB segregation of Au.

energy has a reasonably lower absolute value than $E_\mathrm{s} = -13.0$ kJ/mol obtained earlier for Au segregation at the surface of a Cu-7.5at.%Au alloy [62].

These two examples demonstrate that separate measurements of s and D_b are now possible for both strongly and weakly segregating impurities. As

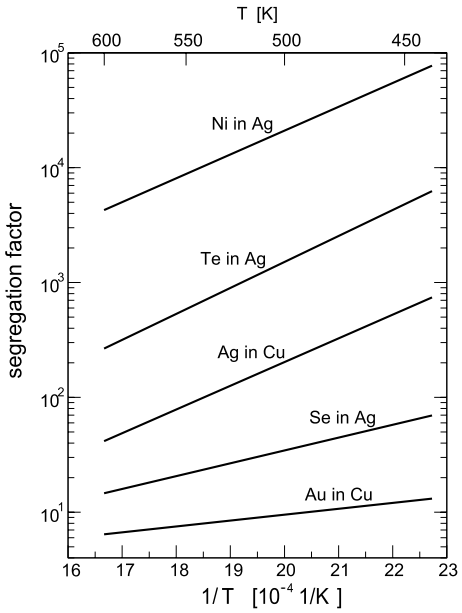

Fig. 8.12. GB segregation factors obtained by combined B and C regime measurements: Te in Ag [56], Au in Cu [57], Se in Ag [58, 59], Ni in Ag [59], and Ag in Cu [60].

mentioned before, such measurements offer the only way to study GB segregation in materials in which direct segregation measurements are hampered by their ductility or tendency to transgranular fracture. Figure 8.12 presents a summary of GB segregation data in other systems obtained by diffusion measurements. We see again that segregation factors can be determined over a wide range spanning almost five orders of magnitude. In all cases studied, GB segregation tends to reduce the GB diffusion rate of the impurity. In particular, impurities which are slow diffusers in the lattice diffuse even slower in GBs, as exemplified by Ni in Ag [59]. Furthermore, a fast diffuser in the lattice may be a slow diffuser in GBs if the segregation level is high enough, e.g. Te in Ag [56]. An atomistic theory explaining this "retardation effect" is yet to come.

8.4.2 Beyond the Linear Segregation

Until this point we assumed that the GB segregation followed a Henry-type isotherm, i.e., that the segregation factor s in (8.4) was a function of temperature only. This approximation is only valid when both the volume concentration $c_{\mathrm{v}}(y,t) = c(\pm\delta/2, y, t)$ and the GB concentration $c_{\mathrm{b}}(y,t)$ of the impurity, expressed in mole fractions with respect to the host element, are small. This condition in turn can only be met when the segregation is not very strong. In systems with a high level of segregation, especially at low temperatures, the GB concentration c_{b} can be relatively large. Then, the GBs can show a tendency to a saturation with the impurity and thus to a non-linear de-

pendence between c_v and c_b. A non-linear dependence means that the ratio $c_\mathrm{b}/c_\mathrm{v}$ in the joining condition (8.4) is no longer constant. Instead, it depends on the volume concentration c_v, and since c_v changes with depth y, the ratio $c_\mathrm{b}/c_\mathrm{v}$ also changes along the penetration profile. The depth dependence of $c_\mathrm{b}/c_\mathrm{v}$ can affect the shape of the penetration profile and should be taken into account in the profile analysis.

This problem was first analyzed by Martin and Perraillon [63] and more recently by Bokshtein et al. [64] and the present authors [65]. All these analyses included the non-linearity of GB segregation by using McLean's isotherm instead of the Henry isotherm. McLean's isotherm of GB segregation has the form

$$c_\mathrm{b} = \frac{sc_\mathrm{v}}{1 + (s-1)c_\mathrm{v}}, \tag{8.30}$$

where s depends only on temperature, $s = s_0 \exp(-E_\mathrm{s}/RT)$. If the volume concentration is small, $c_\mathrm{v} \to 0$, then (8.30) reduces to the Henry isotherm, $c_\mathrm{b} = sc_\mathrm{v}$. If c_v is large, (8.30) gives $c_\mathrm{b} \to 1$, meaning that the GB is saturated with the impurity.

Using the approximations introduced by Fisher [3], the basic equations of the model can be solved analytically. For a constant source, we obtain the following expression for c_b as a function of the reduced depth w:

$$w = \pi^{1/4} \int_{\sigma c_\mathrm{b}}^{\sigma c_0} \frac{\mathrm{d}c}{[-2\ln(1-c) - 2c]^{1/2}}. \tag{8.31}$$

Here $\sigma \equiv (s-1)/s$ and c_0 is the surface concentration. The average concentration measured in sectioning experiments equals

$$\overline{c} = 2\int_0^\infty c(x,y,t)\mathrm{d}x = 4\left(\frac{Dt}{\pi}\right)^{1/2} \cdot c_\mathrm{v} = 4\left(\frac{Dt}{\pi}\right)^{1/2} \cdot \frac{c_\mathrm{b}}{s-(s-1)c_\mathrm{b}}. \tag{8.32}$$

We thus have two functions, $w = w(c_\mathrm{b})$ given by (8.31) and $\overline{c} = \overline{c}(c_\mathrm{b})$ given by (8.32), which define the penetration profile $\overline{c}(w)$ parametrically.

Typical penetration profiles $\log \overline{c}/\overline{c}_0$ versus w calculated from (8.31) and (8.32) are shown in Fig. 8.13, $\overline{c}_0$ being the surface value of the average concentration $\overline{c}$. The profiles consist of two parts:

1. The GB saturation region ($w < 1$) in which $\overline{c}$ rapidly decreases and the profile has a strong upward curvature. In this region the GB concentration remains almost constant, $c_\mathrm{b} \approx 1$, while the volume concentration c_v drops rapidly.

2. The linear-segregation region ($w > 1$) in which the profile is consistent with Fisher's exponential solution, (8.8). In this region both c_v and c_b are small and the linear segregation isotherm is a good approximation. It is this part of the profile that can be used for the determination of $s\delta D_\mathrm{b}$ using standard methods of profile analysis.

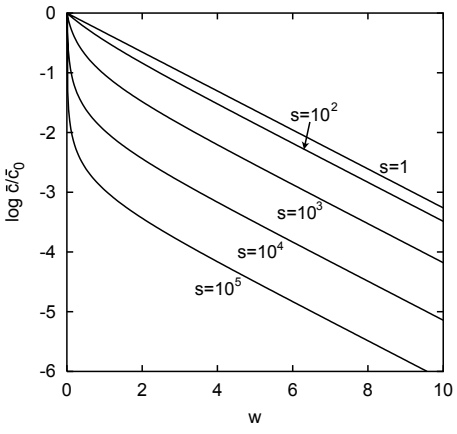

Fig. 8.13. Typical GB penetration profiles calculated with McLean's isotherm [65].

The profile shape shown in Fig. 8.13 is rather general and could be obtained by using more accurate mathematical solutions of the model or other forms of the non-linear isotherm of segregation. With more accurate solutions, the linear-segregation part of the profile has a slight downward curvature according to the $w^{6/5}$-approximation.

Examples of experimental profiles measured for a strongly segregating impurity and containing two steps are available in the literature. Although it seems tempting to immediately explain the near-surface part of such profiles by the solute-saturation effect, one should bear in mind that the near-surface region of the profiles can be affected by many other factors, such as direct volume diffusion from the surface, diffusion along dislocations, GB motion, etc.

In order to avoid such complications, GB diffusion measurements in well-oriented bicrystals offer a convenient way of studying the effect of non-linear segregation. This has been demonstrated in a recent investigation of Ag GB diffusion in Cu bicrystals near the $\Sigma = 5(310)[001]$ orientation [66]. A curved penetration profile similar to those presented in Fig. 8.13 has been measured for Ag GB diffusion (Fig. 8.14, circles), whereas a perfectly linear, type-B profile has been measured for Au GB diffusion in the same bicrystal (squares). Because Au diffusion closely represents Cu self-diffusion (very low segregation, cf. Fig. 8.12), the difference in the shape of the profiles can be directly attributed to the strong GB segregation of Ag in Cu and the associated effect of GB saturation near the surface. Further details of this study can be found in [66].

8.5 Conclusion

Diffusion along GBs is a phenomenon of both practical importance and significant fundamental interest. Modern GB diffusion studies employ novel ex-

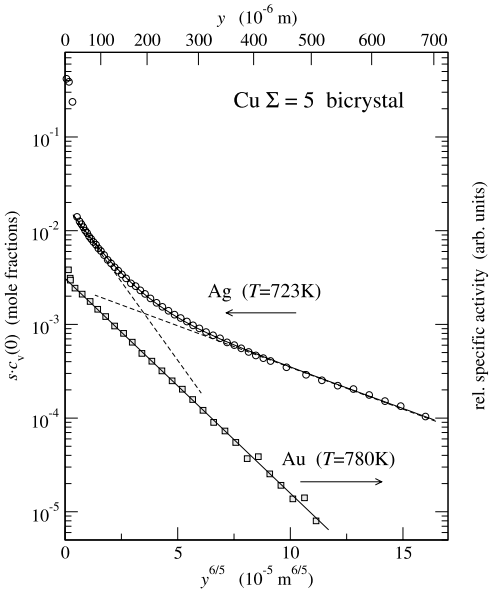

Fig. 8.14. Experimental demonstration of non-linear segregation of Ag in Cu. The concentration profiles have been measured for Ag (circles, left axis) [66] and Au (squares, right axis) [37] GB diffusion in a Cu bicrystal near the $\Sigma = 5(310)[001]$ orientation. The measured specific radioactivity of the ^{110m}Ag tracer has been recalculated to the absolute concentration of Ag (in mole fractions). $c_v(0)$ is the Ag bulk concentration in lattice regions adjacent to the GB and s is the GB segregation factor measured under dilute limit conditions in [60].

perimental techniques for precise radiotracer measurements combined with elaborate mathematical treatments of the experimental profiles. The large volume of experimental data accumulated to date follows clear systematics and provides a reasonably good understanding of GB diffusion, at least on a phenomenological level. One of the most impressive achievements in this area is the implementation of GB diffusion measurements at relatively low temperatures in the C-regime. Such measurements, combined with traditional measurements in the B regime, open the long awaited possibility of separate determination of the GB diffusion coefficient D_b and the impurity segregation factor s.

GB diffusion measurements can be used as a tool to study other properties of GBs, such as their structure, migration, impurity segregation, etc. Since GB diffusion is sensitive to GB structure and chemistry and because radiotracer experiments do not practically disturb the initial state of GBs, diffusion measurements provide useful information on the structural and chemical state of GBs. The importance of this capability is emphasized by the fact that, in contrast to an open surface, GBs are buried interfaces, which makes their studies more difficult. Cleavage of a material along GBs may strongly disturb the initial state of the GBs and in addition is not feasible for many materials. High-resolution transmission electron microscopy is probably the most effective technique for GB studies, but it involves some other problems which will not be discussed here. In this situation, GB diffusion measurements can serve as a useful complimentary technique to study GB properties averaged over a 10^{-4} m length scale (typical penetration length along GBs).

In what follows we will briefly discuss a few other interesting topics that have not been addressed here in detail.

Grain boundary diffusion and segregation in solid solutions: GB diffusion in a binary solution A-B depends on tracer diffusion coefficients of both components in the volume and in GBs, as well as the respective GB segregation factors. In contrast to impurity diffusion, all these quantities generally depend on the bulk composition. There are systems in which both components have suitable radiotracers and their diffusion characteristics can thus be established as functions of the bulk composition. However, there is only one system, Fe-Sn [67], in which both GB diffusion coefficients and segregation factors were determined by independent measurements. In all other systems (e.g. Ag-Sn [68], Ag-Ni [69]) only the products $(s\delta D_{\mathrm{b}})_{\mathrm{A}}$ and $(s\delta D_{\mathrm{b}})_{\mathrm{B}}$ were determined, and not s_{A} and s_{B} separately, which makes the interpretation of the results very difficult. Now that a separate determination of D_{b} and s is possible, it seems timely to revisit some of those systems and determine the composition dependencies of both diffusion and segregation characteristics of A and B over a range of temperatures and compositions.

Grain boundary diffusion in intermetallic compounds: GB diffusion data in ordered intermetallics are scarce. Meanwhile, the need for such data is rapidly growing, especially for transition metal aluminides in view of their potential applications as high temperature structural materials. Intermetallics are also suitable model systems to study the effect of bulk ordering and non-stoichiometry on GB diffusion. The compounds in which GB diffusion has been measured include Ni_3Al [70–72], NiAl [73, 74], Ti_3Al [73, 74], TiAl [73, 74], Fe_3Al [75], FeCo [75], Ni_2Si [77], Ni_2Si_5 [78], $CoSi_2$ [78], and NiSb [79]. While Al and Si diffusion measurements are hampered by the lack of suitable isotopes, diffusion of the transition element does not present a particular problem. In most Ni and Ti aluminides and in FeCo, the ratio Q_{b}/Q lies within the same range 0.4–0.6 as in pure metals, whereas in silicides Q_{b}/Q is anomalously high, 0.7–0.9. Ti diffusion in Ti_3Al also shows unusually high Q_{b}/Q values varying between 0.68 (which is a borderline value) for the stoichiometric composition and 0.88 for the 35 at.%Al alloy.

Tôkei et al. [75] have studied the effect of a bulk phase transition on GB diffusion of Fe in Fe_3Al and Fe and Co in FeCo. In FeCo, GB diffusion shows a discontinuity near the temperature of the bulk order-disorder transition. In contrast, in Fe_3Al GB diffusion does respond to the order-disorder transition. This difference was tentatively explained by a partial atomic order around GBs in Fe_3Al pertaining even above the bulk transition temperature, but this interesting hypothesis requires an atomic level verification.

The effect of non-stoichiometry on GB diffusion has been studied in Ni and Ti aluminides [70, 71, 73, 74]. In Ni_3Al [70, 71], Ni GB diffusion has a minimum at the ideal stoichiometry and increases with deviations from the stoichiometry on either side. In Ti_3Al [73, 74], the measurements have only been performed on the Al-rich side, and Ti GB diffusion has been found to

decrease with the bulk Al concentration. Interestingly, in both compounds bulk diffusion of Ni and Ti almost does not depend on the composition, suggesting that the observed composition dependence of GB diffusion is due to local effects such as GB segregation and/or disorder. On the other hand, the data available for the equiatomic compounds NiAl and TiAl do not indicate any composition dependence of GB diffusion [73, 74]. It appears that more measurements and theoretical work need to be done in this area before any understanding can be reached.

Diffusion in moving grain boundaries: Under real conditions GBs often move as a result of recrystallization, grain growth, and other processes. Moreover, GB diffusion itself is capable of making otherwise stationary GBs move in a random manner. The diffusion induced GB migration (DIGM) is only observed during interdiffusion, i.e., when a substantial amount of foreign atoms is diffused into the sample [80]. Although the nature of DIGM is still not well-understood, many GB diffusion experiments have probably been affected by DIGM. Even during a radiotracer self-diffusion experiment in a well-annealed polycrystalline sample some GBs can still move due to the continued grain growth and/or the trend to establish equilibrium inclination angles between GBs and the surface. GB migration can have a noticeable effect on the shape of the measured concentration profiles and should be taken into account in their analysis. It has been shown that GB motion only modifies a near-surface part of the profile whereas the tail of the profile is not affected. Thus, from the shape of the entire profile measured in the B regime we can determine not only the product $s\delta D_{\mathrm{b}}$ for stationary GBs but also the average velocity v of moving GBs [81]. Again, diffusion measurements can be used as a tool to study the kinetics of GB migration [82]. The first experimental study of this type was performed for self-diffusion in α-Hf [83] and was followed by similar studies of Co and Ni impurity diffusion in Nb [84–86]. An interesting observation in [83] is that the activation energy of GB migration, 195 ± 18 kJ/mol, evaluated from the temperature dependence of v, is close to the measured activation energy of self-diffusion along stationary GBs, 212 ± 9 kJ/mol. This result can be interpreted as evidence that the activation barrier for atomic transport *across* GBs during their migration is essentially the same as the barrier of the atomic transport *along* GBs.

Atomistic theory of grain boundary diffusion: Much progress has been recently achieved in the atomistic interpretation of GB diffusion through computer modeling. The atomistic computer simulations have employed many-body interatomic potentials and a variety of simulation methods, see e.g. [25–29]. It has been recognized that, in contrast to lattice diffusion, GB diffusion is accompanied by strong and temperature dependent correlations between successive atomic jumps [87]. Analysis of jump correlation effects is thus a prerequisite for the understanding of the diffusion-structure relationship in GBs. It has also been established that GBs support both vacancies and interstitials, but these defects can show interesting structural effects such

as vacancy delocalization, vacancy instability at certain cites in the GB core, etc. [26, 27]. Vacancies can move in GBs by single-atom exchanges, like in a regular lattice, but can also make collective jumps involving several atoms. Interstitial formation energies in GBs are close to vacancy formation energies, which makes both defects equally important for diffusion. Interstitials can be either localized or form split dumbbell configurations. They move predominantly by the interstitialcy mechanism involving 2-4 atoms. A challenging problem in this area is to calculate GB diffusion characteristics as functions of misorientation between the two grains, particularly around a low-Σ orientation for which experimental data are available or can be measured.

Notation

bcc	body-centered cubic
c	diffusant concentration in the volume
c_b	diffusant concentration in the grain boundary
c_0	constant course concentration
$\overline{c}$	average concentration of the diffusant measured by the serial sectioning technique
D	volume diffusion coefficient
D_b	grain boundary diffusion coefficient
D_b0	pre-exponential factor of grain boundary diffusion
D_eff	effective diffusion coefficient in a polycrystalline material
d	spacing between grain boundaries in a polycrystalline material
DIGM	diffusion induced grain boundary migration
E_s	segregation energy
fcc	face-centered cubic
f	volume fraction of grain boundaries in a polycrystalline material
h	thickness of the initial layer of diffusant
hcp	hexagonal close-packed
ISOLDE	isotope separator on-line detector
L	diffusion penetration depth in the volume
L_b	diffusion penetration depth along grain boundaries
ln	natural logarithm (on base e)
log	common logarithm (on base 10)
M	amount of diffusant deposited per unit area of the surface
Q	activation energy of volume diffusion
Q_b	activation energy of grain boundary diffusion
R	gas constant
s	segregation factor
T	absolute temperature
T_m	melting temperature
t	diffusion anneal time
v	grain boundary migration velocity

w	reduced coordinate along the diffusion direction
α	diffusion parameter
β	diffusion parameter
δ	grain boundary width
θ	tilt angle
Λ	kinetic parameter of the A regime
Σ	reciprocal density of coincident site in the grain boundary

References

1. R.S. Barnes: Nature **166**, 1032 (1950)
2. A.D. Le Claire: Phil. Mag. **42**, 468 (1951)
3. J.C. Fisher: J. Appl. Phys. **22**, 74 (1951)
4. I. Kaur, Y. Mishin, W. Gust: *Fundamentals of Grain and Interphase Boundary Diffusion* (Wiley, Chichester West Sussex 1995)
5. Y. Mishin, Chr. Herzig, J. Bernardini, W. Gust: Intern. Mater. Reviews **42**, 155 (1997)
6. Y. Mishin, Chr. Herzig: Mater. Sci. Eng. A **260**, 55 (1999)
7. Y. Mishin: Defect Diffus. Forum **194-199**, 1113 (2001)
8. I. Kaur, W. Gust, L. Kozma: *Handbook of Grain and Interphase Boundary Diffusion Data* (Ziegler, Stuttgart 1989)
9. T. Suzuoka: Trans. Jap. Inst. Metals **2**, 25 (1961)
10. T. Suzuoka: J. Phys. Soc. Japan **19**, 839 (1964)
11. Y.M. Mishin, I.M. Razumovskii: Acta Metall. Mater. **40**, 597 (1992)
12. R.T.P. Whipple: Phil. Mag. **45**, 1225 (1954)
13. S.J. Rothman: The measurement of tracer diffusion coefficients in solids. In: *Diffusion in Crystalline Solids*, ed by G.E. Murch, A.S. Nowick (Academic Press, New York 1984) p 1
14. J. Philibert: *Atom Movements – Diffusion and Mass Transport in Solids* (Les Éditions de Physique, Les Ulis 1991)
15. H.S. Levine, C.J. MacCallum: J. Appl. Phys. **31**, 595 (1960)
16. A.D. Le Claire: Brit. J. Appl. Phys. **14**, 351 (1963)
17. Y.M. Mishin: Phys. Stat. Solidi (a) **133**, 259 (1992)
18. B.S. Bokshtein, I.A. Magidson, I.L. Svetlov: Phys. Met. Metallogr. **6**, 81 (1958)
19. G.B. Gibbs: Phys. Status Solidi **16**, K 27 (1966)
20. A.P. Sutton, R.W. Balluffi: *Interfaces in Crystalline Materials* (Clarendon Press, Oxford 1995)
21. *Materials Interfaces. Atomic-Level Structure and Properties*, ed by D. Wolf, S. Yip (Chapman & Hall, London 1992)
22. J.M. Howe: *Interfaces in Materials* (Wiley, New York 1997)
23. J. Sommer, Chr. Herzig: J. Appl. Phys. **72**, 2758 (1992)
24. P. Gas, D.L. Beke, J. Bernardini: Phil. Mag. Lett. **65**, 133 (1992)
25. Y. Mishin: Defect Diffus. Forum **143–147**, 1357 (1997)
26. M.R. Sørensen, Y. Mishin, A.F. Voter: Phys. Rev. B **62**, 3658 (2000)
27. A. Suzuki, Y. Mishin: Interface Sci. **11**, 131 (2003)
28. P. Keblinski, D. Wolf, S.R. Phillpot, H. Gleiter: Phil. Mag. A **79**, 2735 (1999)
29. P. Keblinski, V. Yamakov: Interface Sci. **11**, 111 (2003)

30. N.A. Gjostein. In: *Diffusion* (Amer. Soc. Metals, Metals Park OH 1974) p 241
31. A.M. Brown, M.F. Ashby: Acta Metall. **28**, 1085 (1980)
32. W. Gust, S. Mayer, A. Bögel, B. Predel: J. de Physique **46**, 537 (1985)
33. R.E. Hoffman: Acta Metall. **4**, 56 (1956)
34. J. Sommer, Chr. Herzig, S. Mayer, W. Gust: Defect Diffus. Forum **66–69**, 843 (1989)
35. D. Turnbull, R.E. Hoffman: Acta Metall. **2**, 419 (1954)
36. E. Budke, Chr. Herzig, S. Prokofjev, L.S. Shvindlerman: Mater. Sci. Forum **207–209**, 465 (1996)
37. E. Budke, T. Surholt, S. Prokofjev, L.S. Shvindlerman, Chr. Herzig: Acta Mater. **47**, 385 (1999)
38. T. Surholt, D. Molodov, Chr. Herzig: Acta Mater. **46**, 5345 (1998)
39. P. Klugkist, A.N. Aleshin, W. Lojkowski, L.S. Shvindlerman, W. Gust, E.J. Mittemeijer: Acta Mater. **49**, 2941 (2001)
40. W.R. Upthegrove, M.J. Sinnot: Trans. ASM **50**, 1031 (1958)
41. Quing Ma, R.W. Balluffi: Acta Metall. Mater. **41**, 133 (1993)
42. R.W. Balluffi: Mechanisms of grain boundary diffusion. In: *Diffusion in Crystalline Solids*, ed by G.E. Murch, A.S. Nowick (Academic Press, New York 1984) p 319
43. Quing Ma, C.L. Liu, J.B. Adams, R.W. Balluffi: Acta Metall. Mater. **41**, 143 (1993)
44. L.G. Harrison: Trans. Faraday Soc. **57**, 1191 (1961)
45. E.W. Hart: Acta Metall. **5**, 597 (1957)
46. I.V. Belova, G.E. Murch: Phil. Mag. A **81**, 2447 (2001)
47. Y. Oishi, H. Ichimura: J. Chem. Phys. **71**, 5134 (1979)
48. N.S. Basu, J.W. Halloran: Oxid. Metals **27**, 143 (1987)
49. W. Wegener, G. Borchardt: Oxid. Metals **36**, 339 (1991)
50. Y. Mishin, Chr. Herzig: Nanostruct. Mater. **6**, 859 (1995)
51. Y. Mishin, I.V. Yurovitskii: Phil. Mag. A **64**, 1239 (1991)
52. V.V. Kondratev, I.S. Trachtenberg: Phys. Status Solidi (b) **171**, 303 (1992)
53. L. Klinger, E. Rabkin: Acta Mater. **47**, 725 (1999)
54. S.V. Divinski, Y.-S. Kang, J.-S. Lee, F. Hisker, Chr. Herzig: Interface Sci. **11**, 67 (2003)
55. Y.-S. Kang, J.-S. Lee, S.V. Divinski, Chr. Herzig: Z. Metallkd. **95**, 76 (2004)
56. Chr. Herzig, J. Geise, Y. Mishin: Acta Metall. Mater. **41**, 1683 (1993)
57. T. Surholt, Y. Mishin, Chr. Herzig: Phys. Rev. **B50**, 3577 (1994)
58. T. Surholt, Chr. Herzig: Mater. Sci. Forum. **207–209**, 481 (1996)
59. T. Surholt, C. Minkwitz, Chr. Herzig: Acta Mater **46**, 1849 (1998)
60. S.V. Divinski, M. Lohman, Chr. Herzig: Defect Diffus. Forum, **194-199**, 1127 (2001)
61. A. Atkinson, R.I. Taylor: Phil Mag. A **43**, 979
62. W. Losch, J. Kirschner: J. Vac. Sci. Technol. **15**, 1541 (1978)
63. G. Martin, B. Perraillon: Measurements of Grain Boundary Diffusion. In: *Grain Boundary Structure and Kinetics*, ed by R. W. Balluffi (Amer. Soc. Metals, Metals Park OH 1980) p 239
64. B.S. Bokshtein, V.E. Fradkov, D.L. Beke: Phil. Mag. A **65**, 277 (1992)
65. Y. Mishin, Chr. Herzig: J. Appl. Phys. **73**, 8206 (1993)
66. S.V. Divinski, M. Lohman, Chr. Herzig: Interface Sci. **11**, 21 (2003)
67. J. Bernardini, P. Gas, E.D. Hondros, M.P. Sea: Proc. Royal Soc. Lond. **A379**, 159 (1982)

68. P. Gas, J. Bernardini: Surf. Sci. **72**, 365 (1978)
69. P. Gas, J. Bernardini. In: *Proc. 18th Int. Congr. Vacuum Technology and Vacuum Metallurgy*, vol 2 (Cannes 1980) p 501
70. S. Frank, J. Rüsing, Chr. Herzig: Intermetallics **4**, 601 (1996)
71. S. Frank, Chr. Herzig: Mater. Sci. Eng. **239-240**, 882 (1997)
72. J. Čermak, I. Stloukal, J. Ruvzikova: Intermetallics **8**, 21 (1998)
73. Chr. Herzig, S.V. Divinski, S. Frank, T. Przeorski: Defect Diffus. Forum **194-199**, 317 (2001)
74. Chr. Herzig, T. Wilger, T. Przeorski, F. Hisker, S.V. Divinski: Intermetallics **9**, 431 (2001)
75. Z. Tôkei, J. Bernardini, D.L. Beke: Acta Mater. **47**, 1371 (1999)
76. J. Bernardini, P. Gas: Defect Diffus. Forum **143-147**, 1343 (1997)
77. J.C. Ciccarriello, S. Poize, P. Gas: J. Appl. Phys. **67**, 3315 (1990)
78. T. Barge, P. Gas, F.M. d'Heurle: J. Mater. Res. **10**, 1134 (1995)
79. R. Hahnel, W. Miekeley, H. Wever: Phys. Status Solidi (a) **97**, 181 (1986)
80. A.H. King: Intern. Metals Reviews **32**, 173 (1987)
81. Y.M. Mishin, I.M. Razumovskii: Acta Metall. Mater. **40**, 839 (1992)
82. Y. Mishin, M. Köppers, Chr. Herzig: Solid State Phenom. **41**, 79 (1995)
83. F. Güthoff, Y. Mishin, Chr. Herzig: Z. Metallkd. **84**, 584 (1993)
84. M. Köppers, Y. Mishin, Chr. Herzig: Acta Metall. Mater. **42**, 2859 (1994)
85. M. Köppers, Y. Mishin, Chr. Herzig: Scr. Metall. Mater. **32**, 1113 (1995)
86. I.M. Razumovskii, Y. Mishin, Chr. Herzig: Mater. Sci. Eng. A **212**, 45 (1996)
87. Y. Mishin: Phil. Mag. A **72**, 1589 (1995)